How to cite: Angew. Chem. Int. Ed. 2024, e202404775
doi.org/10.1002/anie.202404775

Heterogeneous Catalysis

Structure and Chemical Reactivity of Y-Stabilized ZrO_2 Surfaces: Importance for the Water-Gas Shift Reaction

Shuang Chen, Philipp N. Pleßow, Zairan Yu, Eric Sauter, Lachlan Caulfield, Alexei Nefedov, Felix Studt, Yuemin Wang, and Christof Wöll**

Abstract: The surface structure and chemical properties of Y-stabilized zirconia (YSZ) have been subjects of intense debate over the past three decades. However, a thorough understanding of chemical processes occurring at YSZ powders faces significant challenges due to the absence of reliable reference data acquired for well-controlled model systems. Here, we present results from polarization-resolved infrared reflection absorption spectroscopy (IRRAS) obtained for differently oriented, Y-doped ZrO_2 single-crystal surfaces after exposure to CO and D_2O. The IRRAS data reveal that the polar YSZ(100) surface undergoes reconstruction, characterized by an unusual, red-shifted CO band at 2132 cm^{-1}. Density functional theory calculations allowed to relate this unexpected observation to under-coordinated Zr^{4+} cations in the vicinity of doping-induced O vacancies. This reconstruction leads to a strongly increased chemical reactivity and water spontaneously dissociates on YSZ(100). The latter, which is an important requirement for catalysing the water-gas-shift (WGS) reaction, is absent for YSZ(111), where only associative adsorption was observed. Together with a novel analysis Scheme these reference data allowed for an operando characterisation of YSZ powders using DRIFTS (diffuse reflectance infrared Fourier transform spectroscopy). These findings facilitate rational design and tuning of YSZ-based powder materials for catalytic applications, in particular CO oxidation and the WGS reaction.

Introduction

Zirconia (ZrO_2) stands out as a crucial oxide material, owing to its distinctive physical and chemical properties characterized by ideal mechanical and chemical stability, outstanding thermal resilience, low thermal expansion coefficient, significant ionic conductivity, and a high refractive index. As a result, ZrO_2 has found extensive applications across various fields, including catalysis,[1] solid-oxide fuel cells (SOFC),[2] structural ceramics,[3] and gas sensors.[4] The monoclinic (m) phase is stable at room temperature (RT), and the transition to tetragonal (t) ZrO_2 occurs when heated to approximately 1447 K. At temperatures exceeding 2650 K, cubic (c) ZrO_2 emerges. Among these phases, the high-temperature c-ZrO_2 is particularly valuable due to its numerous technological applications compared to m- and t-ZrO_2.[5] Pure c- ZrO_2 exhibits instability at room temperature but can be rendered stable through doping with rare earth oxides, typically Y_2O_3.[6]

The surface structure of Y-stabilized ZrO_2 (YSZ) plays a crucial role, particularly in catalytic applications. One of the most important reactions is the water-gas shift (WGS) reaction, in which this oxide shows activity even without adding co-catalysts like transition metals.[7] Previous theoretical work has proposed a mechanism for the WGS reaction on zirconia surfaces, highlighting the crucial importance of hydroxyl groups and water dissociation.[8] However, experimental reference data on single crystals to validate these theoretical findings is lacking. It is somewhat unclear how hydroxyl groups are created; zirconia is generally considered to be rather inert towards water, as demonstrated by studies on zirconia thin films.[9]

Herein, we present a polarization-resolved infrared reflection absorption spectroscopy (IRRAS) investigation on various YSZ (9.5 mol % Y_2O_3) single-crystal surfaces using the CO surface ligand IR (CO-SLIR) approach.[10] Since no other IRRAS studies of CO on zirconia single crystals have been reported, the assignment of CO vibrations was aided by density functional theory (DFT) calcu-

[*] Dr. S. Chen, Z. Yu, Dr. E. Sauter, L. Caulfield, Dr. A. Nefedov, Dr. Y. Wang, Prof. Dr. C. Wöll
Institute of Functional Interfaces (IFG)
Karlsruhe Institute of Technology (KIT)
76344 Eggenstein-Leopoldshafen (Germany)
E-mail: yuemin.wang@kit.edu
christof.woell@kit.edu

Dr. P. N. Pleßow, Prof. Dr. F. Studt
Institute of Catalysis Research and Technology (IKFT)
Karlsruhe Institute of Technology (KIT)
76344 Eggenstein-Leopoldshafen (Germany)

Prof. Dr. F. Studt
Institute for Chemical Technology and Polymer Chemistry (ICTP)
Karlsruhe Institute of Technology (KIT)
Engesserstrasse 18, 76131 Karlsruhe (Germany)

lations. For the polar YSZ(100) surface, an unusual low-lying band at 2132 cm^{-1} was identified and assigned to the low-coordinated surface Zr^{4+} sites in the vicinity of doping-induced O vacancies. These special Zr^{4+}-ions sites, characterized by a red-shifted CO vibration, are crucial for the chemical reactivity of this polar surface in low-temperature water dissociation. For CO adsorbed on YSZ(111), only a single CO band was detected at 2169 cm^{-1}, showing a blue shift typical for oxide surfaces.[11] Following previous work on ZrO_2 powders, this band is attributed to CO bound to Zr^{4+} sites.[12]

Exposing the single-crystal YSZ(111) surface to water (D_2O) at 75 K resulted in the formation of mono- and multilayers of intact water; no hydroxy species were observed. In pronounced contrast, annealing YSZ(100) led to the occurrence of two distinct OD species at 2723 and 2706 cm^{-1}, demonstrating substantial chemical activity on this polar zirconia surface.

The accurate reference data acquired for differently oriented YSZ substrates allows for an unambiguous identification of adsorbate species on YSZ powders using diffuse reflectance infrared Fourier transform spectroscopy (DRIFTS). The DRIFTS data demonstrates that, unexpectedly, (100) facets of YSZ particles are reduced at atmospheric pressures of CO even at room temperature.

Results and discussion

Studies on YSZ single crystals

Polarization-resolved IRRAS, employing CO as a probe, allows for an appropriate monitoring of the atomic structure of oxide surfaces. We note that the interaction of dielectric materials with IR radiation is notably more intricate than in case of metals. The so-called "surface selection rule"[13] does not apply to oxidic substrates.[11] As shown in Figure S1, the sign and intensity of the vibrational bands of adsorbates depend strongly on the interaction between the transition dipole moment (TDM) and the IR incident light involving different components: p-polarized light parallel ($E_{p,t}$) and perpendicular ($E_{p,n}$) to the substrate surface, as well as s-polarized component (E_s).[11] Figure 1a displays the polarization-resolved IRRAS results obtained after saturation adsorption of CO on YSZ(100) at 70 K. The p-polarized spectrum is dominated by an intense IR band at 2132 cm^{-1}, which must be related to CO adsorbed on surface Zr^{4+} ions. The second, weaker signal at 2162 cm^{-1} is tentatively assigned to CO bound at surface Y^{3+} species. This assignment is in full accord with the results of DFT calculations (see below) and with reference data recorded under ultra-high vacuum (UHV) conditions in IR transmission for CO adsorbed on Y_2O_3 powders (Figure S2), where the surface Y^{3+}-related CO vibration is observed at 2166 cm^{-1}. In the IRRAS data recorded with s-polarized light (Figure 1a) no vibrational signals were detected, indicating that all CO species adopt a nearly upright adsorption geometry. For reduced YSZ(100) surfaces prepared by annealing in UHV at 770 K, a new IR signal emerged at about 2085 cm^{-1}

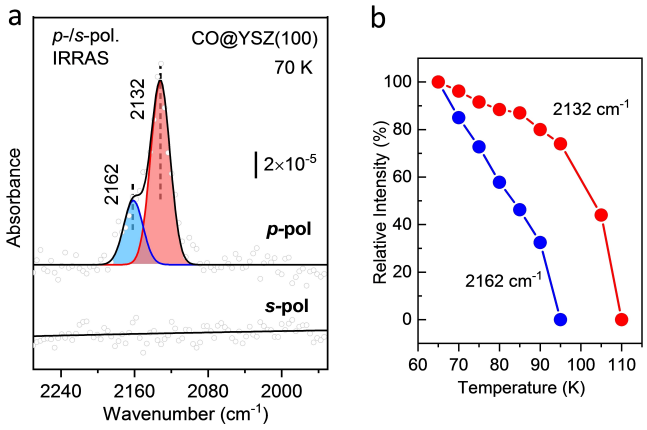

Figure 1. Polarization-resolved IRRAS characterization of the structural and electronic properties of YSZ single crystal surfaces. a) p- and s-polarized IRRA spectra recorded after CO adsorption (10 L) on YSZ(100) at 70 K with a grazing incidence of 80°. b) Relative intensity (peak area) of CO species adsorbed on YSZ(100) as a function of sample temperature.

(Figure S3). This red shift of CO bands upon reduction has been seen for other oxides as well and is explained by enhanced π-backdonation from reduced $Zr^{\delta+}$-sites to adsorbed CO.[14]

Importantly, the Zr^{4+}-related CO band for YSZ(100) exhibits a lower frequency (2132 cm^{-1}), which is red-shifted compared to the gas phase value of 2143 cm^{-1}. This observation is in pronounced contrast to other oxidic substrates, where fully oxidized surfaces typically show a blue shift in CO adsorbate vibrational frequencies (e.g., CeO_2,[15] ZnO,[16] TiO_2,[17] and ZrO_2[12]). We relate the unexpected red shift of the CO vibration on the polar YSZ(100) surface to the distinctive chemical environments of surface Zr^{4+} cations. In comparison to the 8-fold coordinated Zr^{4+} in zirconia bulk, the surface Zr^{4+} on YSZ(100) is significantly under-coordinated. In addition, the presence of O-vacancies (resulting from doping with Y^{3+} ions) is expected to cause further changes in chemical activity. These hypotheses are fully confirmed by the DFT calculations, as shown below.

We would like to point out that the unique structural and electronic properties of YSZ(100) result in an unexpected sign reversal of the CO vibrational bands (Figure 1a, Figure S3). In contrast to the negative CO band observed on YSZ(111) (Figure S1) and all previously reported IRRAS data for CO on oxide single crystal surfaces,[11,15–17] the vibrational bands here appear as positive signals in the absorption spectra. A similar sign reversal has been observed for NO adsorbed on TiO_2(110) upon reducing the substrate.[18] Analysis using the classical three-phase mode for dielectric materials (Figure S4),[19] reveals that the positive sign observed for CO bound to YSZ(100) is directly associated with a change of the refractive index n, originating from the surface reduction induced by O-vacancy doping.

The temperature-dependent IRRAS data allows us to estimate the binding energy of various CO species adsorbed

on YSZ(100) (Figure S3b). Upon annealing, the CO coverage decreases due to gradual desorption, leading to a slight blue shift in all peaks to higher wavenumbers: $\Delta\nu = +8\ cm^{-1}$ for CO-Y^{3+} and $\Delta\nu = +12\ cm^{-1}$ for CO-Zr^{4+}. This coverage-induced frequency shift is attributed to repulsive lateral interactions between CO adsorbates, involving both dynamic and substrate-mediated static interactions.[16b] Concurrently, the CO-Y^{3+} and CO-Zr^{4+} species undergo a gradual attenuation and disappear at about 95 and 110 K, respectively. Figure 1b provides a quantitative analysis of the CO desorption IRRAS data, displaying the relative intensity (peak area) as a function of sample temperature. This analysis, based on the deconvoluted IRRAS data shown in Figure S5, yielded binding energies of 28 ± 2 kJ/mol (0.29 ± 0.02 eV) for CO-Y^{3+} and of 32 ± 2 kJ/mol (0.33 ± 0.02 eV) for CO-Zr^{4+}, respectively.

The chemical reactivity of the YSZ(100) surface was assessed using IRRAS for the water dissociation reaction. Notably, the TDM of O-H(D) stretching vibrations on oxide single-crystal surfaces is extremely weak, rendering IRRAS observation a challenging and intricate task.[20] Figure 2a and b show the p- and s-polarized IRRAS data recorded after exposing the YSZ(100) surface to 5 L of D_2O at 116 K, followed by heating to the indicated temperatures. The p-polarized spectra are dominated by a broad negative band centered at 2525 cm^{-1}, which is assigned to the intermolecular H-bonds oriented normal to the surface coupling with $p_{n,z}$-polarized light (perpendicular to the surface, see Figure S1). This reveals the formation of H-bonded 3D water multilayer structures. The sharp OD vibration at 2729 cm^{-1} is characteristic of the non-H-bonded ("dangling") OD groups of terminal D_2O molecules.[20] Strong H-bond interactions within the D_2O multilayers are further demonstrated by the presence of two low-lying IR bands at 2436 and 2354 cm^{-1}, observed in both p-polarized (positive sign) and s-polarized IRRAS (negative sign). These broad OD vibrations, marked by polarization-dependent sign reversal, arise from intermolecular H-bonds oriented parallel to the surface. They interact with both $p_{t,x}$-polarized and s-polarized light, thus resulting in positive and negative OD bands, respectively.

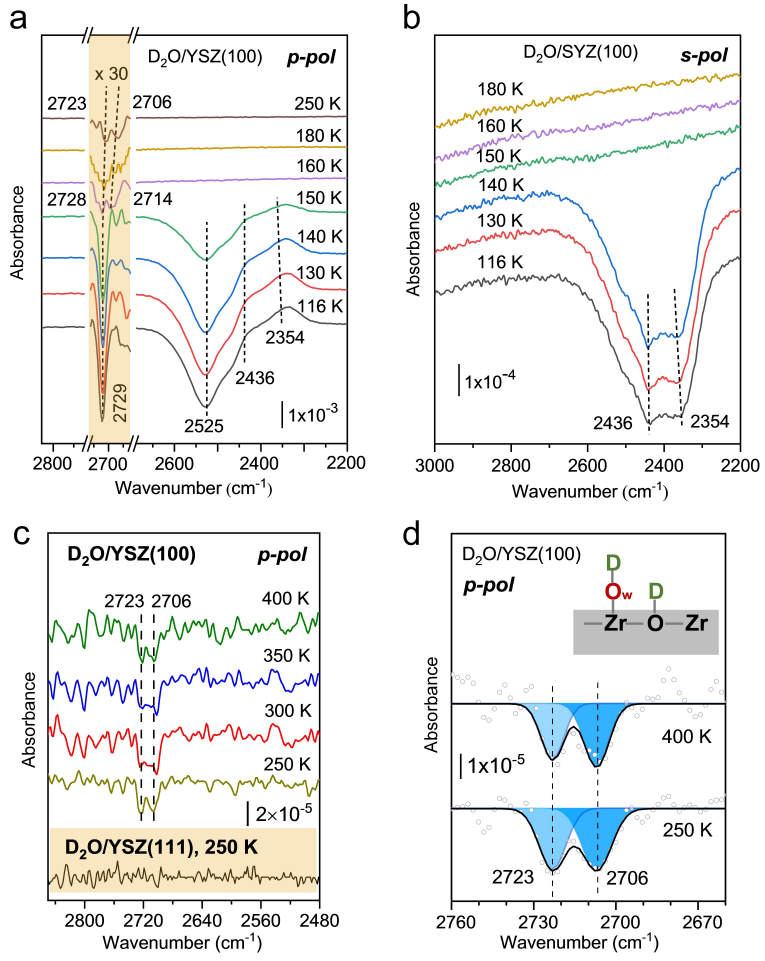

Figure 2. Chemical reactivity of the YSZ(100) surface towards low-temperature water dissociation tracked by IRRAS. a) p-polarized and b) s-polarized IRRAS data obtained after adsorption of 5 L D_2O on the YSZ(100) surface at 116 K and gradually heating to 250 K. c) p-polarized IRRAS data obtained after adsorption of 5 L D_2O on the YSZ(100) surface at 116 K and subsequently heating to 250, 300, 350, and 400 K. d) Deconvoluted IRRA spectra at 250 and 400 K. For comparison, the corresponding IRRAS data of D_2O on YSZ(111) at 250 K is shown in c).

The temperature-dependent IRRAS data in Figure 2a,b show complete desorption of multilayer water upon annealing to 160 K. Importantly, the desorption of D_2O molecules is accompanied by the appearance of two sharp OD vibrations at 2706 and 2723 cm^{-1} in p-polarized IRRAS (Figure 2c). Both signals are thermally stable and remain nearly unchanged after annealing in UHV to 400 K (Figure 2d), revealing the formation of two different hydroxyl species via water dissociation. The intensity of both bands decreases significantly as the sample temperature rises to 450 K. The two peaks are respectively assigned to an O_sD species formed via hydrogen transfer to a substrate O atom (O_s), and an O_wD-group attached to a substrate Zr^{4+} cation, as shown in the inset of Figure 2d. Notably, these OD vibrational signals were not detected in the s-polarized IRRAS, indicating that, for both OD groups, the TDM is mainly oriented perpendicular to the surface.

In pronounced contrast, the YSZ(111) surface exhibited only molecular adsorption of water at low temperatures, with no OD species emerging upon annealing (see Figure 2c). This observation is in line with previous temperature programmed desorption (TPD) studies on ZrO_2(111) thin films.[9]

Studies on powders

Building upon the reference data for CO adsorbate frequencies acquired for YSZ single-crystal surfaces, we extended our investigations to commercial YSZ powders (8 mol % Y_2O_3, Alfa Aesar) using in situ UHV-FTIRS (IR transmission) and high-pressure DRIFTS.

The cubic fluorite-type structure of YSZ powders was confirmed by the characteristic X-ray diffraction (XRD) pattern observed in Figure S6. Scanning electron microscopy (SEM) images (Figure S7) revealed particle sizes ranging from several tens to one hundred nm, with the particles exposing facets of different crystallographic orientations. Figure 3 and Figure S8. summarize the IR results obtained using three different IR methods on YSZ, encompassing both well-defined single crystals and nanoparticles across a wide range of CO pressures (from 10^{-10} mbar to 1 bar) and temperatures (65 K to 295 K). The in situ UHV-FTIRS (10^{-3} mbar at 65 K, Figure 3c) and DRIFTS (1 bar at 295 K, Figure 3d) results consistently show a predominant blue-shifted band at 2170–2180 cm^{-1} originating from CO-Zr^{4+} species primarily located on the energetically most favourable {111}-facets. In addition, a weak signal is detected at 2132 cm^{-1} resulting from CO bound to {100}-facets. The 2170 cm^{-1} band is in agreement with that (2169 cm^{-1}) of CO adsorbed to the YSZ(111) surface (Figure 3b), while the

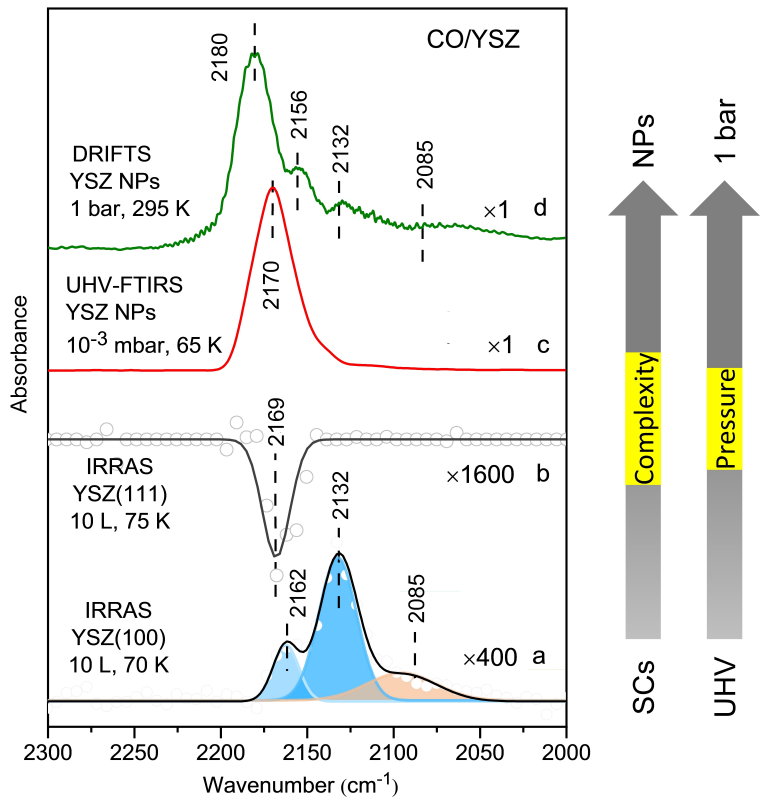

Figure 3. IR investigations (polarization-resolved IRRAS, in situ UHV-FTIRS, high-pressure DRIFTS) on YSZ single crystals and powders across a broad range of pressures and temperatures. (a,b) p-polarized IRRAS data of CO saturation adsorption: a) on the reduced YSZ(100) single crystal surface at 70 K; b) on the YSZ(111) single crystal surface at 75 K. c) In situ IR transmission (UHV-FTIR) spectra of CO adsorption on YSZ powders in a CO pressure of 10^{-3} mbar at 65 K. d) In situ difference DRIFTS data of CO adsorption on YSZ powders in a CO pressure of 1 bar at 295 K. SCs: single-crystals; NPs: nanoparticles; UHV: ultrahigh vacuum.

slight deviation observed in DRIFTS (2180 cm^{-1}, Figure 3d) is attributed to the coverage-induced frequency shift. The latter was also evident in the temperature-dependent IR data, where the CO vibrational frequency shifts from 2170 to 2198 cm^{-1} during CO desorption at higher temperatures (Figure S9). The weak band at 2156 cm^{-1} is characteristic of CO bound to acidic hydroxyl groups via hydrogen bonding.[21]

It is widely recognized that in situ/operando DRIFT spectra of CO primarily exhibit intense and broad gas-phase rovibrational signals centered at approximately 2170 cm^{-1} (R-branch) and 2120 cm^{-1} (P-branch), posing challenges for a reliable observation and identification of CO vibrations on catalyst surfaces.[22] In this work, we effectively eliminated the CO gas-phase contribution using a novel normalization/subtraction scheme,[23] where DRIFT spectra of both the reference (KBr) and YSZ powders were recorded at a high-resolution of 2 cm^{-1} (Figure S10). Briefly, the YSZ and KBr spectra were initially normalized, followed by subtracting the KBr reference data from the YSZ data. More importantly, the high-quality DRIFTS data clearly reveal a new IR feature at about 2085 cm^{-1} that increases in intensity with prolonged exposure to 1 bar CO at 295 K (see Figure S8). On the basis of the IRRAS data obtained for the YSZ(100) surface (Figure 3a), this band is assigned to CO adsorbed to surface $Zr^{\delta+}$ sites. These results demonstrate that the CO-induced reduction of surface Zr^{4+} cations occurs even at low temperatures (295 K).

Theoretical results

The adsorption and vibrational frequencies of CO on YSZ(100) were investigated by employing DFT at the PBE–D3[24] level of theory using the PAW method as implemented in VASP 5.4.1,[25] symmetric slab models with varying concentrations of Y and according amounts of oxygen vacancies were constructed (overall formula $Zr_nY_{2m}O_{2n+3m}$). Low amounts of doping generally lead to significant reconstruction of the surface. Stable surfaces were obtained with 50 % Y in the first two layers, where (1x1x5)-layered slabs were employed, see Figure 4a, d. The distribution of Y in the top two layers is also the most stable arrangement for this Y:Zr composition. The oxygen vacancies are positioned in the first and second layer. The remaining oxygen ions sometimes occupy intermediate position between the bulk positions expected in the first and second layer.

The adsorption of CO on YSZ(100) was studied for $\theta = 1/2$ and $\theta = 1/8$ monolayer (1 ML corresponds to one CO per surface metal atom, see Figure 4b,c,e,f). The adsorption energies on Zr (Y) are similar with −0.54 (−0.59) eV at $\theta = 1/2$ ML and −0.83 (−0.83) eV at $\theta = 1/8$ ML. For CO-Zr^{4+} the calculated frequency shift relative to free CO is $\Delta\nu = -14$ cm^{-1} (2129 cm^{-1}) at $\theta = 1/2$ ML (Figure 4b,e) and $\Delta\nu = -11$ cm^{-1} (2132 cm^{-1}) at $\theta = 1/8$ ML, whereas for CO-Y^{3+} a blue-shift in frequency was observed with $\Delta\nu = +17$ cm^{-1} (2160 cm^{-1}) at $\theta = 1/2$ ML (Figure 4c,f) and $\Delta\nu = +20$ cm^{-1} (2163 cm^{-1}) at $\theta = 1/8$ ML. The computed frequencies and the corresponding coverage-induced shift for both CO

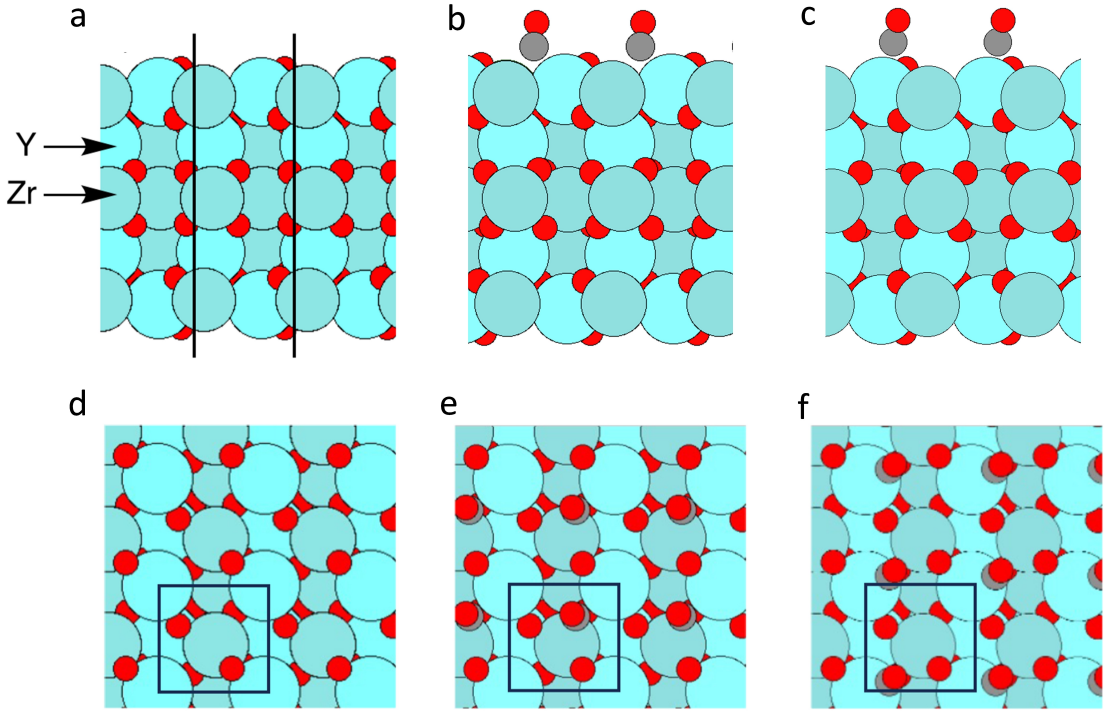

Figure 4. DFT optimized structures of pure and CO-adsorbed YSZ(100) surfaces. (a–c) side views of (a) pure YSZ(100), (b) CO adsorbed to surface Zr^{4+}, and (c) CO adsorbed to surface Y^{3+}; (d–f) top views of (d) pure YSZ(100), (e) CO adsorbed to surface Zr^{4+}, and (f) CO adsorbed to surface Y^{3+}. Surface unit cells are indicated.

species agree well with the experimental assignment. For CO/YSZ(111), we obtain a blue-shift of $\Delta\nu = +12\ cm^{-1}$ ($2155\ cm^{-1}$) for CO adsorbed to surface Zr^{4+} of undoped ZrO_2(111) at $\theta = 1/4$ ML and a wider spread, but mostly blue-shifts for Y^{3+}-doped surfaces (see Figure S11).

Since in recent work it has been found that frequency calculations for CO adsorbed on oxides using PBE functionals may be inaccurate,[15d,26] we performed additional calculations using the hybrid HSE06 functional (see Figure S11). The results reveal that for the zirconia substrates investigated here the differences in frequency are so small that they can be neglected.

Conclusion

In summary, we presented the first polarization-resolved IRRAS study elucidating the surface structure and chemical reactivity of YSZ single crystal surfaces. While the results obtained for the YSZ(111) are mostly consistent with previous work on zirconia thin films,[9] a number of unexpected observations were made for CO and D_2O interacting with the polar YSZ(100) surface. This polar surface undergoes reconstruction and exposes under-coordinated Zr^{4+} cations stabilized by adjacent O vacancies. These surface Zr^{4+} species are characterized by an unusual red-shifted CO stretching vibration at $2132\ cm^{-1}$. In addition, the YSZ(100) surface shows high activity in low-temperature water dissociation. It was found that CO-induced reduction occurs on (100) facets of YSZ powders even at room temperature under ambient CO pressures (1 bar). These findings shed light on the unique surface properties of YSZ(100) and hold significant implications for an atomic-level understanding of the surface structure and active sites of YSZ-based catalysts, especially in the context of low-temperature CO oxidation and WGS reactions.

Acknowledgements

This work was funded by the Deutsche Forschungsgemeinschaft (DFG, German Research Foundation)—Project-ID 426888090—SFB 1441. S.C. is grateful for a Postdoc fellowship donated by the Helmholtz Association and China Postdoctoral Council (OCPC). P.N.P. and F.S. acknowledge support by the state of Baden-Württemberg through bwHPC (bwunicluster and JUSTUS, RV bw17D011) and the German Research Foundation (DFG) through grant no INST 40/575-1 FUGG (JUSTUS 2 cluster). Open Access funding enabled and organized by Projekt DEAL.

Conflict of Interest

The authors declare no conflict of interest.

Data Availability Statement

The data that support the findings of this study are available in the supplementary material of this article.

Keywords: Density functional theory · IRRAS · Surface chemistry · YSZ · ZrO_2

[1] a) E. Aneggi, V. Rico-Perez, C. Leitenburg, S. Maschio, L. Soler, J. Llorca, A. Trovarelli, *Angew. Chem. Int. Ed.* **2015**, *54*, 14040–14043; b) X. Zhang, H. Shi, B. Q. Xu, *Angew. Chem. Int. Ed.* **2005**, *44*, 7132–7135; c) X. Chen, H. Y. Zhu, J. C. Zhao, Z. F. Zheng, X. P. Gao, *Angew. Chem. Int. Ed.* **2008**, *47*, 5453–5456; d) M. Allan, D. Grinter, S. Dhaliwal, C. Muryn, T. Forrest, F. Maccherozzi, S. S. Dhesi, G. Thornton, *Surf. Sci.* **2019**, *682*, 8–13; e) Y. Wang, G. Wang, L. I. van der Wal, K. Cheng, Q. Zhang, K. P. de Jong, Y. Wang, *Angew. Chem. Int. Ed.* **2021**, *60*, 17735–17743.

[2] a) B. Stolten, B. Emonds, Fuel Cell Science and Engineering, Wiley-VCH: Weinheim, **2012**; b) K. T. Lee, A. A. Lidie, H. S. Yoon, E. D. Wachsman, *Angew. Chem. Int. Ed.* **2014**, *53*, 13463–13467; c) S. Volkov, V. Vonk, N. Khorshidi, D. Franz, M. Kubicek, V. Kilic, R. Felici, T. M. Huber, E. Navickas, G. M. Rupp, J. Fleig, A. Stierle, *Chem. Mater.* **2016**, *28*, 3727–3733; d) Y. Song, S. Zhou, Q. Dong, Y. Li, X. Zhang, N. Ta, Z. Liu, J. Zhao, F. Yang, G. Wang, X. Bao, *Angew. Chem. Int. Ed.* **2019**, *58*, 4617–4621.

[3] C. Piconi, G. Maccauro, *Biomaterials* **1999**, *20*, 1–25.

[4] C. Lopez-Gandara, F. M. Ramos, A. Cirera, A. Cornet, *Sens. Actuators B* **2009**, *140*, 432–438.

[5] a) E. D. Wachsman, K. T. Lee, *Science* **2011**, *334*, 935–939; b) G. Korotcenkov, S. D. Han, J. R. Stetter, *Chem. Rev.* **2009**, *109*, 1402–1433; c) Y. Han, J. F. Zhu, *Top. Catal.* **2013**, *56*, 1525–1541; d) M. Richard, F. Can, D. Duprez, S. Gil, A. Giroir-Fendler, N. Bion, *Angew. Chem. Int. Ed.* **2014**, *53*, 11342–11345; e) M. N. Tsampas, F. M. Sapountzib, P. Vernoux, *Catal. Sci. Technol.* **2015**, *5*, 4884–4900.

[6] a) P. Duwez, F. H. Brown, F. Odell, *J. Electrochem. Soc.* **1951**, *98*, 356; b) E. V. Stefanovich, A. L. Shluger, C. R. A. Catlow, *Phys. Rev. B* **1994**, 11560–11571.

[7] a) C. Ratnasamy, J. P. Wagner, *Catal. Rev.* **2009**, *51*, 325–440; b) J. H. Carter, X. Liu, Q. He, S. Althahban, E. Nowicka, S. J. Freakley, L. Niu, D. J. Morgan, Y. Li, J. W. Niemantsverdriet, S. Golunski, C. J. Kiely, G. J. Hutchings, *Angew. Chem. Int. Ed.* **2017**, *56*, 16037–16041.

[8] a) M. L. Cerón, B. Herrera, P. Araya, F. Gracia, A. Toro-Labbé, *J. Mol. Model.* **2013**, *19*, 2885–2891; b) S. Kouva, J. Andersin, K. Honkala, J. Lehtonen, L. Lefferts, J. Kanervo, *Phys. Chem. Chem. Phys.* **2014**, *16*, 20650–20664; c) D. T. Chaopradith, D. O. Scanlon, C. R. A. Catlow, *J. Phys. Chem. C* **2015**, *119*, 22526–22533.

[9] P. Lackner, J. Hulva, E. M. Köck, W. Mayr-Schmölzer, J. I. J. Choi, S. Penner, U. Diebold, F. Mittendorfer, J. Redinger, B. Klötzer, G. S. Parkinson, M. Schmid, *J. Mater. Chem. A* **2018**, *6*, 17587–17601.

[10] C. Wöll, *ACS Catal.* **2019**, *10*, 168–176.

[11] Y. Wang, C. Wöll, *Chem. Soc. Rev.* **2017**, *46*, 1875–1932.

[12] S. Kouva, K. Honkala, L. Lefferts, J. Kanervo, *Catal. Sci. Technol.* **2015**, *5*, 3473–3490.

[13] R. G. Greenler, *J. Chem. Phys.* **1966**, *44*, 310–315.

[14] a) C. Morterra, E. Giamello, L. Orio, M. Volante, *J. Phys. Chem.* **1990**, *94*, 3111–3116; b) J. P. Goff, W. Hayes, S. Hull, M. T. Hutchings, K. N. Clausen, *Phys. Rev. B* **1999**, *59*, 14202–14219; c) J. Zhu, S. Albertsma, J. G. V. Ommen, L. Lefferts, *J. Phys. Chem. B* **2005**, *109*, 9550–9555.

[15] a) C. Yang, L. L. Yin, F. Bebensee, M. Buchholz, H. Sezen, S. Heissler, J. Chen, A. Nefedov, H. Idriss, X. Q. Gong, C. Wöll, *Phys. Chem. Chem. Phys.* **2014**, *16*, 24165–24168; b) C. Yang, X. Yu, S. Heißler, A. Nefedov, S. Colussi, J. Llorca, A. Trovarelli, Y. Wang, C. Wöll, *Angew. Chem. Int. Ed.* **2017**, *56*, 375–379; c) C. Yang, M. Capdevila-Cortada, C. Dong, Y. Zhou, J. Wang, X. Yu, A. Nefedov, S. Heissler, N. Lopez, W. Shen, C. Wöll, Y. Wang, *J. Phys. Chem. Lett.* **2020**, *11*, 7925–7931; d) G. Lustemberg, P. N. Plessow, Y. Wang, C. Yang, A. Nefedov, F. Studt, C. Wöll, M. V. Ganduglia-Pirovano, *Phys. Rev. Lett.* **2020**, *125*, 256101.

[16] a) Y. Wang, X. Y. Xia, A. Urban, H. S. Qiu, J. Strunk, B. Meyer, M. Muhler, C. Wöll, *Angew. Chem. Int. Ed.* **2007**, *46*, 7315–7318; b) M. Buchholz, X. Yu, C. Yang, S. Heissler, A. Nefedov, Y. Wang, C. Wöll, *Surf. Sci.* **2016**, *652*, 247–252.

[17] a) M. C. Xu, Y. K. Gao, E. M. Moreno, M. Kunst, M. Muhler, Y. Wang, H. Idriss, C. Wöll, *Phys. Rev. Lett.* **2011**, *106*, 138302; b) M. C. Xu, H. Noei, K. Fink, M. Muhler, Y. Wang, C. Wöll, *Angew. Chem. Int. Ed.* **2012**, *51*, 4731–4734; c) M. Setvin, M. Buchholz, W. Y. Hou, C. Zhang, B. Stoger, J. Hulva, T. Simschitz, X. Shi, J. Pavelec, G. S. Parkinson, M. C. Xu, Y. Wang, M. Schmid, C. Wöll, A. Selloni, U. Diebold, *J. Phys. Chem. C* **2015**, *119*, 21044–21052.

[18] M. C. Xu, Y. K. Gao, Y. Wang, C. Wöll, *Phys. Chem. Chem. Phys.* **2010**, *12*, 3649–3652.

[19] a) W. N. Hansen, *J. Opt. Soc. Am.* **1968**, *58*, 380–390; b) W. N. Hansen, *Symp. Faraday Soc.* **1970**, *4*, 27–35; c) J. A. Mielczarski, R. H. Yoon, *J. Phys. Chem.* **1989**, *93*, 2034–2038.

[20] a) L. Schöttner, R. Ovcharenko, A. Nefedov, E. Voloshina, Y. Wang, J. Sauer, C. Wöll, *J. Phys. Chem. C* **2019**, *123*, 8324–8335; b) X. Yu, P. Schwarz, A. Nefedov, B. Meyer, Y. Wang, C. Wöll, *Angew. Chem. Int. Ed.* **2019**, *131*, 17915–17921.

[21] a) K. I. Hadjiivanov, G. N. Vayssilov, *Adv. Catal.* **2002**, *47*, 307–511; b) A. Vimont, J.-M. Goupil, J.-C. Lavalley, M. Daturi, S. Surblé, C. Serre, F. Millange, G. Férey, N. Audebrand, *J. Am. Chem. Soc.* **2006**, *128*, 3218–3227; c) J. Wang, W. Wang, Z. Fan, S. Chen, A. Nefedov, S. Heißler, R. A. Fischer, C. Wöll, Y. Wang, *J. Phys. Chem. C* **2021**, *125*, 593–601.

[22] a) A. Paredes-Nunez, I. Jbir, D. Bianchi, F. C. Meunier, *Appl. Catal. A* **2015**, *495*, 17–22; b) C. Meunier, *J. Phys. Chem. C* **2021**, *125*, 21810–21823.

[23] L. Caulfield, E. Sauter, H. Idriss, Y. Wang, C. Wöll, *J. Phys. Chem. C* **2023**, *127*, 14023–14029.

[24] a) J. P. Perdew, K. Burke, M. Ernzerhof, *Phys. Rev. Lett.* **1996**, *77*, 3865–386; b) S. Grimme, J. Antony, S. Ehrlich, H. Krieg, *J. Chem. Phys.* **2010**, *132*, 154104.

[25] a) P. E. Blöchl, *Phys. Rev. B* **1994**, *50*, 17953–17979; b) G. Kresse, J. Furthmuller, *Phys. Rev. B* **1996**, *54*, 11169–11186; c) G. Kresse, D. Joubert, *Phys. Rev. B* **1999**, *59*, 1758–1775.

[26] P. Lustemberg, C. Yang, Y. Wang, C. Wöll, V. Ganduglia-Pirovano, *J. Chem. Phys.* **2023**, *159*, 034704.

Manuscript received: March 11, 2024
Accepted manuscript online: May 17, 2024
Version of record online: ■■, ■■

Research Articles

Heterogeneous Catalysis

S. Chen, P. N. Pleßow, Z. Yu, E. Sauter, L. Caulfield, A. Nefedov, F. Studt, Y. Wang,* C. Wöll* _____ e202404775

Structure and Chemical Reactivity of Y-Stabilized ZrO_2 Surfaces: Importance for the Water-Gas Shift Reaction

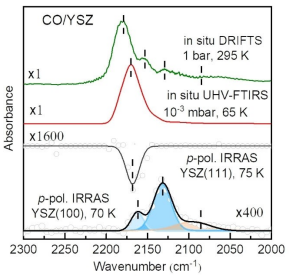

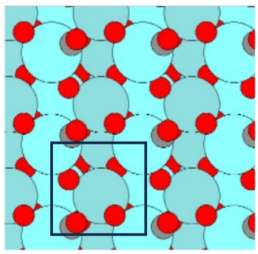

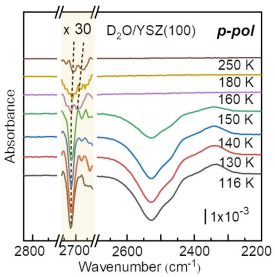

We present a systematic IR spectroscopic study on Y-stabilized ZrO_2 (YSZ) in the form of both well-defined single-crystals (polarization-resolved IRRAS) and nanoparticles (in situ IR transmission, high-pressure DRIFTS) with a special focus on the polar YSZ(100) surface and its interactions with CO and D_2O. The IR results in conjunction with DFT calculations demonstrate that this surface is characterized by low-coordinated Zr^{4+} cations in the presence of O vacancies generated by Y^{3+}-doping, showing superior activity for low-temperature water dissociation.